DIRECT NUMERICAL SIMULATIONS OF TURBULENT FLOW OVER MOVING SINUSOIDAL BOUNDARIES

Peter P. Sullivan*, James C. McWilliams†, and Chin-Hoh Moeng
National Center for Atmospheric Research, Boulder, CO

ABSTRACT

Turbulent flow over idealized water waves is investigated using direct numerical simulations at a bulk Reynolds number $Re = 8000$ over non-evolving water waves with varying waveslope ak and wave age c/u_*. The results show that waves significantly influence the mean flow, vertical momentum fluxes, velocity variances, pressure, and form stress (drag). Compared to a stationary wave, slow (fast) moving waves increase (decrease) the form stress. A region of closed streamlines (or cat's-eye pattern) centered about the critical layer height was observed at low to moderate values of c/u_* and was found to be dynamically important in determining the mean flow, turbulent fluxes, and surface form stress.

INTRODUCTION

Our understanding of the physical mechanisms at work in air-sea interaction remains elusive because of the formidable difficulties of obtaining and interpreting field observations over the open ocean, *e.g.*, Edson and Fairall (1998). From the perspective of the atmospheric boundary layer, questions persist as to the influence of ocean waves on the height of the wave induced boundary layer, the partitioning of the vertical momentum flux between turbulent and wave induced components, the modification of Monin-Obukhov similarity theory, and the role wave age plays in the determination of surface drag.

There is an extensive body of literature on flow over waves both experimental and computational using second-order closures (*e.g.*, see Belcher and Hunt (1998) for a review), and a few turbulence resolving simulations above stationary roughness (*e.g.*, Cherukat et al., 1998). The direct numerical simulations described in this work serve as a precursor for more geophysically realistic large-eddy simulations over finite amplitude waves to be considered in the future.

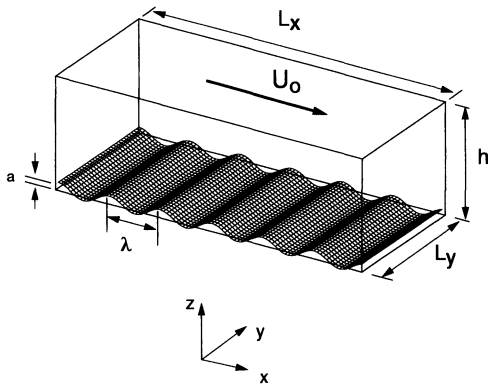

Figure 1: Sketch of 3D Couette flow driven by velocity U_o over a moving wavy boundary of wavelength λ (wavenumber $k = 2\pi/\lambda$), phase speed c, amplitude a, and waveslope $ak = a2\pi/\lambda$ in a domain of size $(L_x, L_y, h) = (6, 5, 1)\lambda$. The surface grid is shown with less resolution than actually used in the computations.

PROBLEM FORMULATION

The problem considered is viscous three-dimensional turbulent Couette flow over two-dimensional water waves. A sketch showing the flow orientation, coordinate system, and the sinusoidal lower boundary is given in Fig. 1. We adopt a coordinate system where x is aligned with the primary flow direction, y is parallel to the wave crests and z is measured vertically from the mean water surface. The corresponding Cartesian velocity components are (u, v, w) and the fluid viscosity and density are (ν, ρ). In our idealization, the water wave is assumed to be a two-dimensional, periodic (in x), non-evolving, deep-water gravity wave. The orbital velocities at the water surface, which are included in the

*corresponding author address: Peter P. Sullivan , National Center for Atmospheric Research, P. O. Box 3000, Boulder, CO 80307-3000; email: pps@ncar.ucar.edu

†Also at Department of Atmospheric Sciences and Institute of Geophysics and Planetary Physics, UCLA, Los Angeles, CA 90095-1565

surface boundary conditions, are assumed to be given by first order wave theory. For our computations and analysis, the frame of reference is tied to the waves and then the water surface displacements and orbital velocities are independent of time. The flow is assumed to be periodic in the horizontal directions (x,y) and is driven by a large scale constant velocity U_o imposed at $z = h$. Velocity and length scales are made dimensionless by U_o and h, respectively.

NUMERICAL METHOD

The numerical method used to solve the continuity, momentum, and scalar transport equations borrows heavily from our experience with large-eddy simulations of geophysical flows (*e.g.,* Sullivan et al., 1996) and the recent developments described by Zang et al. (1994). In order to accommodate curved boundaries, the usual staggered grid arrangement has been replaced by a cell-centered arrangement for all variables. We use a momentum-interpolation procedure similar to that in Rhie and Chow (1983). This method has been used successfully in Reynolds-averaged closure calculations, but its performance for turbulence simulations is relatively recent (*e.g.,* Zang et al., 1994).

For the specific problem considered, the conservation equations for mass, momentum, and scalar transport are first transformed into computational space using the simple conformal (thus orthogonal) transformation

$$\begin{bmatrix} \xi \\ \eta \\ \zeta \end{bmatrix} = \begin{bmatrix} x - iae^{-kz}e^{ikx} \\ y \\ z - ae^{-kz}e^{ikx} \end{bmatrix} \qquad (1)$$

proposed by Benjamin (1959). Here (ξ,η,ζ) are surface fitted coordinates roughly aligned with the Cartesian (x,y,z) coordinates. $\zeta = 0$ corresponds to the lower boundary of the physical surface. The metric elements connecting the Cartesian and curvilinear systems $\partial\xi_i/\partial x_j$ are written in closed form using (1). The continuity equation and the advective terms in the momentum and scalar transport equations are written in strong conservation form.

In our present direct numerical simulation (DNS) code with a cell-centered arrangement, the spatial differencing remains pseudo-spectral along transformed horizontal coordinates and second-order finite-difference in the transformed vertical direction while the time advancement is a three stage Runge-Kutta scheme. The velocity and pressure are determined by a fractional step method which determines the pressure so that at each new time level the incompressibility constraint is enforced. Variable coefficients appear in the Poisson equation for pressure which requires an iterative solution method.

Table 1: Simulation Properties

ak	c	c/u_*	$u_* \times 10^2$	D_p/u_*^2	κ	z_o^+
0	0	0	3.13	0	0.41	0.17
0.1	0	0	3.21	0.129	0.41	0.22
0.1	0.125	3.91	3.20	0.181	0.35	0.60
0.1	0.25	7.84	3.19	0.124	0.34	0.71
0.1	0.365	11.5	3.17	0.022	0.39	0.26
0.1	0.50	16.2	3.08	-0.016	0.35	0.39
0.1	0.70	22.7	3.08	-0.035	0.37	0.27
0.2	0.25	7.32	3.42	0.262	0.34	1.47

RESULTS

For our turbulence simulations, we consider cases with different values of a and c, including one with a flat, stationary boundary ($a = c = 0$). A summary of the bulk simulation properties is given in Table 1 which lists the waveslope ak, dimensionless phase speed c, wave age c/u_*, the nondimensional friction velocity u_*, form stress D_p/u_*^2, von Kármán constant κ, and dimensionless roughness length z_o^+. We choose the Reynolds number sufficiently large ($Re = U_o h/\nu = 8000$) so that the turbulence is fully developed. The corresponding wall Reynolds number $Re_* = u_* h/2\nu \approx 130$. Our bulk Reynolds number is well beyond the transitional value ($Re \approx 2000$). The number of gridpoints employed is $(N_x,N_y,N_z) = (144,96,96)$ which is adequate to capture the dissipation range at our Reynolds number. The vertical spacing varies from 1.0 to 5.5 in wall units $\Delta\zeta^+ = \Delta\zeta u_*/\nu$. Velocity and length scales normalized by wall variables, *i.e.,* $(1/u_*,\nu/u_*)$, are indicated by $(\,)^+$.

Flow Visualization

Figure 2 is a visualization of the total fluctuating horizontal velocity (wave correlated u_w plus turbulent u' components) in an $x-y$ plane near the surface for flow over a flat boundary and two cases with moving wavy walls, *viz.,* $(c/u_*,ak) = (7.8,0.1)$ and $(c/u_*,ak) = (22.7,0.1)$. We observe that waves drastically alter the near surface flow patterns. The near wall streaky structure, prevalent in flat wall boundary layers, is disrupted by the waves. Wave pumping leads to small pockets of positive and negative fluctuating velocity with horizontal length scales roughly equal to $\lambda/2$ which becomes more pronounced as the wave speed c increases relative to the wind speed. A similar effect is observed in the vertical velocity field w and consequently the instantaneous turbulent flux fields are also modified by the presence of waves.

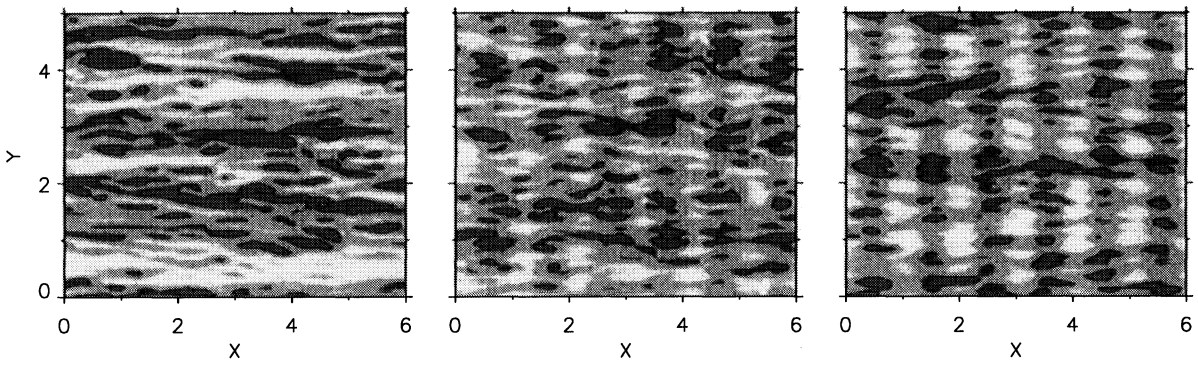

Figure 2: Fluctuating velocity $(u_w + u')/u_*$ in horizontal planes near the the lower boundary $\zeta^+ = 5.2$; left panel flat case; middle panel $(c/u_*, ak) = (7.8, 0.1)$; and right panel $(c/u_*, ak) = (22.7, 0.1)$. Color scheme varies from light to dark corresponding to the range $[-3.5, 3.18]$.

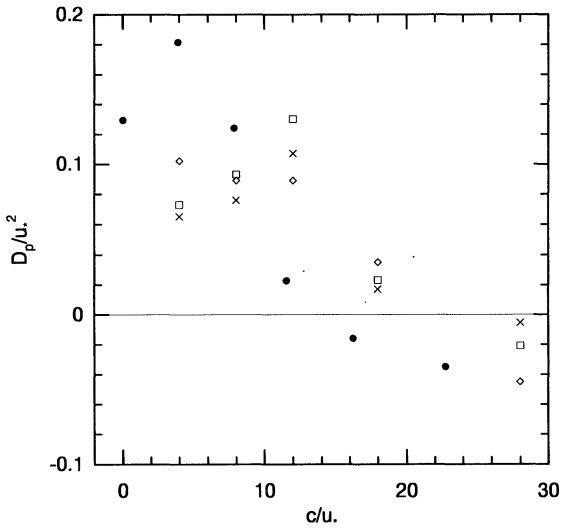

Figure 3: Surface form stress, normalized by u_*^2, for several values of c/u_* and $ak = 0.1$. Values from our DNS are marked with solid dots, and the open symbols indicate values from three different turbulence closure calculations by Li *et al.*(1999), *viz.*, $E - \kappa z$ (□ symbols), $q^2 l$ (◇) , and Launder-Reece-Rodi (×) turbulence models.

Surface Drag

We computed the surface form stress (drag)

$$D_p = \frac{1}{\lambda} \int_0^\lambda p \frac{dz_{bdy}}{dx} dx \,, \qquad (2)$$

where p is the surface pressure and dz_{bdy}/dx is the surface slope. The results are shown in Fig. 3 as function of wave age c/u_* at fixed waveslope $ak = 0.1$. The maximum normalized form stress D_p/u_*^2 is slightly less than 19%. At small c/u_*, the form stress is positive and acts in concert with the viscous stress to decelerate the flow near the wall, while at large c/u_* an opposite trend is observed; the surface form stress is negative and acts as a thrust in opposition to the surface viscous stress. The critical value of c/u_* that marks this transition occurs at $c/u_*|_{tr} \approx 14$. For comparison, the results from various second-order closure calculations are also shown. Our DNS calculations are similar in magnitude, but clearly suggest a smaller $c/u_*|_{tr}$ than the turbulence closure calculations. The calculations of Li et al. (1999) assume the lower surface is aerodynamically rough and the flow is Reynolds number independent so that the mean velocity profile is presumably logarithmic right down to the water surface. Both Reynolds number and surface roughness are known to influence the form drag (Harris et al., 1996; Gent and Taylor, 1976). Categorizing the flow by wave age, either as slow moving waves $c/u_* < c/u_*|_{tr}$ (with positive form stress) or fast moving waves $c/u_* > c/u_*|_{tr}$ (with negative form stress), is useful for interpreting the results to be presented later.

Mean Velocity Profiles

The effect of moving water waves on the mean velocity profiles is one of the open questions in air-sea interaction. Does the presence of moving waves modulate the near surface flow leading to departures from the usual log-law variation over a solid stationary surface ? In order to address this issue, we compared the mean velocity profiles from our simulations to the log-law

$$u^+ = \frac{1}{\kappa} \ln z^+ + b \equiv \frac{1}{\kappa} \ln \frac{z^+}{z_o^+} \equiv \frac{1}{\kappa} \ln \frac{z}{z_o}. \qquad (3)$$

This log-linear variation was assumed to apply to all profiles starting at $z^+ > 25$. A least-squares curve fit of the profiles determined κ and b, and hence $z_o^+ = e^{-\kappa b}$. We estimate the error bar associated with determining

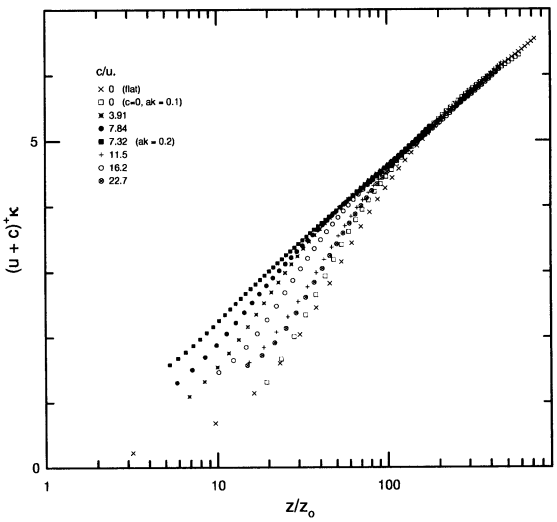

Figure 4: Vertical profiles of mean velocity for flow over moving waves of varying c/u_* and ak at $Re_* = 130$.

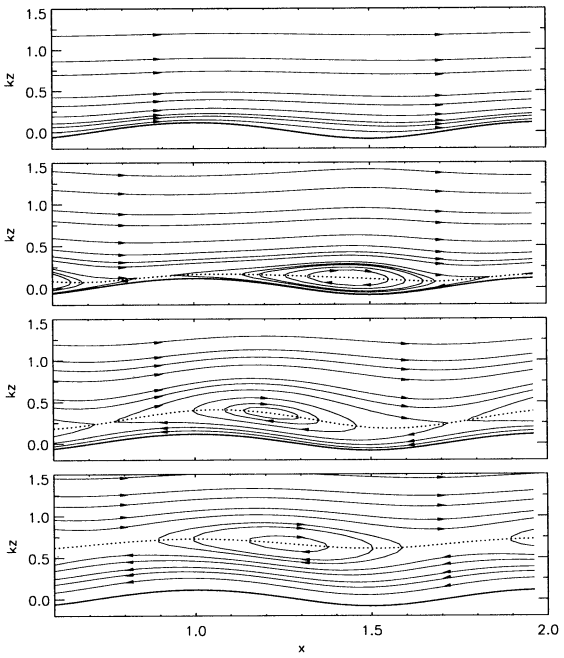

Figure 5: Phase averaged streamlines over stationary and moving waves with $ak = 0.1$ in surface fitted coordinates: upper, $c/u_* = 0$; upper middle, $c/u_* = 3.9$; lower middle, $c/u_* = 7.8$; lower, $c/u_* = 11.5$. The dotted line corresponds to the height of the critical layer where $\langle u \rangle + u_w = 0$.

κ, b, and z_o^+ to be quite small.

The results in Table I indicate that the effect of waves on the roughness length z_o^+ is quite pronounced. Given the relatively small variation in κ, our results show that the change in z_o^+ with wave age is dominated by changes in the log-law intercept b. The utility of z_o^+ is its basis for classifying the sea surface condition. For example, Kitaigorodskii and Donelan (1984) propose the following broad classification of the sea surface state: $z_o^+ \approx 0.1$ smooth, $0.1 < z_o^+ < 2.2$ transitional, and $z_o^+ > 2.2$ fully rough. Based on the above criterion, the surface conditions in the present simulations are in the low to middle transitional regime except for case $(c/u_*, ak) = (7.32, 0.2)$ that just approaches the bottom of the fully rough regime. Since our predicted z_o^+ lies in the transitional regime the current low-Reynolds number DNS simulations are potentially relevant to the geophysical regime.

We found a strong link between roughness length and wave age; slow moving waves are characterized by large z_o^+ (large positive form drag) while fast moving waves have small z_o^+ (small negative form drag) consistent with the results in Fig. 3. The complicating influences of moving waves is further illustrated if we compare z_o^+ over a smooth flat surface with case $(c/u_*, ak) = (22.8, 0.1)$. Surprisingly, z_o^+ is only slightly greater in the presence of finite amplitude fast moving waves indicating that the lower surface in this case is nearly as *smooth* as flow over a flat boundary (see also Hsu and Hsu, 1983).

In Fig. 4, vertical profiles of the mean horizontal velocity in log-linear coordinates are displayed for varying c/u_*. (Note the dimensionless phase speed is included in the mean profiles, z is measured from the mean water surface, and the constants κ and z_o^+ are taken from Table I.) All the profiles collapse to the log-linear variation beyond $z/z_o > 100$. Below $z/z_o < 100$ the profile variation depends on wave age and wave slope. The general trend is that cases with larger z_o^+ display a shorter buffer region and longer logarithmic regions. Notice that for case $(c/u_*, ak) = (7.3, 0.2)$, the velocity profile is near log-linear starting from the crests of the waves indicative of its approach to the fully rough regime.

Critical Layer Dynamics

In order to isolate the mean wave-induced flow fields ensemble and phase averaging operators (*e.g.*, see Hsu et al., 1981) were applied to the velocity components. The resulting velocity field thus consists of ensemble means $(\langle u \rangle, \langle w \rangle)$, which are functions of ζ, and wave correlated components (u_w, w_w), which vary with both (ξ, ζ). The phase averaged vectors $(\langle u \rangle + u_w, \langle w \rangle + w_w)$ are shown as streamlines in Fig. 5 for several different

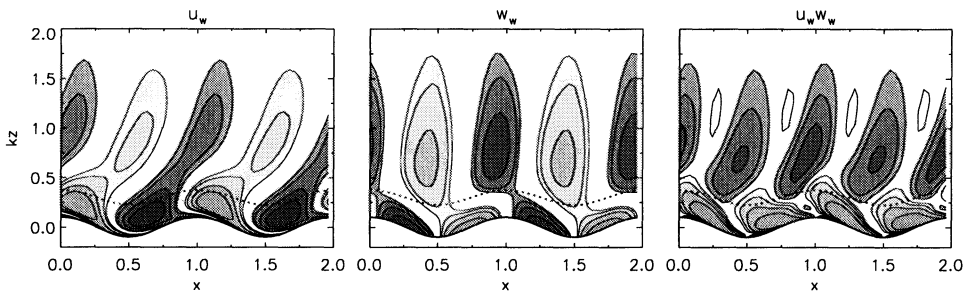

Figure 6: Contours of normalized wave correlated fields. Contours progress from darker to lighter shading with negative (positive) values for the light (dark) shaded family: contour values for u_w/u_* $(\pm 0.2, \pm 0.3, \pm 0.5, \pm 0.7)$, w_w/u_* $(\pm 0.15, \pm 0.2, \pm 0.3, \pm 0.5)$, and flux $u_w w_w/u_*^2$ $(\pm 0.02, \pm 0.05, \pm 0.1, \pm 0.2)$. The dotted line is the critical layer height.

values of c/u_* including the reference case $c/u_* = 0$.

The streamline patterns over moving waves differ from their stationary counterparts in dynamically important ways. Viewed in the frame of reference moving with the waves, the average flow near the surface must be opposite in direction to the primary flow aloft for nonzero c/u_*. A measure of the vertical extent of the reversed flow region is the critical layer height z_{cr} (*e.g.,* Belcher and Hunt (1998)) defined as the vertical location where the total streamwise velocity is identical to zero, *i.e.,* where $\langle u \rangle + u_w = 0$. For given ak, z_{cr} depends on c/u_* and x. At low c/u_*, z_{cr} is generally small $z_{cr} < 0.1/k$ and is strongly asymmetrical about x, being thinner on the windward side of the wave and thicker on the leeward side. At moderate $c/u_* = 7.8$, z_{cr} is higher, tends to follow the wave shape and there is less asymmetry compared to the case with lower c/u_*. Finally, for fast moving waves $z_{cr} > 0.5/k$ and is nearly flat, independent of x.

The structure and importance of the critical layer in flow over moving waves has been the subject of much analysis (see *e.g.,* Miles, 1957; Lighthill, 1962). A consequence of the critical layer is that a region of closed streamlines or "cat's-eyes" must occur if there is any periodic variation of the mean flow along the wave, *e.g.,* Lighthill sketches a symmetrical cat's-eye pattern directly over the wave crest. In the present DNS, the phase averaged cat's-eye pattern at low c/u_* hugs the lower boundary with its center located just upwind of the wave trough ($x \approx 1.4$) and extends nearly over the entire wavelength. Notice also that directly above the center of the cat's-eye pattern the flow is displaced vertically and no longer follows the wavy lower boundary. In other words, for slow moving waves ($c/u_* < 11$) the region of closed streamlines, which encompasses relatively slow moving fluid, acts similar to an obstacle to the fast moving flow above z_{cr} (*i.e.,* the outer flow) deflecting the outer mean streamlines away from the moving wavy surface. Meanwhile, in the case of fast moving waves ($c/u_* > 11$) the critical height is well above the surface and nearly independent of x and thus the cat's-eye pattern only slightly perturbs the near surface streamlines which closely follow the wave shape. Since z_{cr} increases rapidly with c/u_* the interaction between the critical layer and the wave quickly diminishes for fast moving waves. The size, shape, and streamwise and vertical location of the mean cat's-eye pattern, from our DNS, are clearly dependent on c/u_*, but overall are centered between the crest and trough and are at least as thick as the wave amplitude a in good agreement with the measurements of Hsu et al. (1981) for slow moving waves.

Wave Correlated Motions

The effect of the critical layer on the nondimensional wave correlated fields $(u_w, w_w)/u_*$ and their fluxes $u_w w_w/u_*^2$ for case $(c/u_*, ak = 7.8, 0.1)$ is next illustrated in Fig. 6. In this figure, we show spatial (x,z) contours of $(u_w, w_w, u_w w_w)$ and their relative orientation to the critical layer height z_{cr}.

Inspection of the w_w contours shows that for $z < z_{cr}$ the effects of the reverse mean flow and the orbital velocity of the water, which varies like $akc \sin kx$, act in concert to produce positive (negative) w_w on the leeward (windward) side of the wave; a variation opposite compared to the stationary case $(c/u_*, ak = 0.0, 0.1)$. Above the critical layer the (x,z) positions of the maximum and minimum w_w occur roughly above the wave crests and troughs. The variation of u_w is more complex than w_w, being more tightly coupled to conditions above and below the critical height. u_w varies more smoothly across z_{cr} than does w_w but the u_w contours exhibit a pronounced downwind tilt. The contours of u_w as well as its streamwise integrated value hint at a minimum

near $kz = 0.5$, which is just above the cat's-eye pattern (see Fig. 5). Above z_{cr}, the streamwise wave correlated u_w maintains the same sign sense as in the stationary case, but with a more exaggerated streamwise bias. Beneath z_{cr}, the wave correlated flux $u_w w_w$ is predominantly negative and decreases (becomes more negative) with increasing c/u_*. For this value of c/u_*, where the effects of the critical layer are important $u_w w_w > 0$ for $z > z_{cr}$ like flow over stationary waves. Our results for $u_w w_w$ are similar to the measurements of Hsu et al. (1981) who show that the wave correlated flux is positive (negative) above (below) the critical layer. The variation of the wave correlated fields adds further support to the speculation that the critical layer, and the formation of a cat's-eye pattern in essence alters the effective shape of the lower boundary that the outer flow sees, *i.e.,* the flow above the critical layer responds to the geometry given by z_{cr}.

CONCLUSIONS

Results from these DNSs show that the height of the wave induced boundary layer extends out to about $kz = O(1)$ from the water surface and that complex coupling between turbulence in the air and wave-induced surface motions occurs dependent on the wave age parameter c/u_*. The proximity of the critical layer to the wave surface and the resulting cat's-eye pattern significantly influences the mean flow patterns, wave correlated fluxes, and surface drag.

Acknowledgments: NCAR is sponsored by the National Science Foundation. A portion of this work was supported by the Office of Naval Research.

REFERENCES

Belcher, S. E. and Hunt, J.: 1998, 'Turbulent flow over hills and waves', *Annual Review of Fluid Mechanics* **30**, 507–538.

Benjamin, T. B.: 1959, 'Shearing flow over a wavy boundary', *J. Fluid Mech.* **6**, 161–205.

Cherukat, P., Na, Y., Hanratty, T. J. and McLaughlin, J. B.: 1998, 'Direct numerical simulation of a fully developed turbulent flow over a wavy wall', *Theor. and Comp. Fluid Dyn.* **11**, 109–134.

Edson, J. and Fairall, C.: 1998, 'Similarity relationships in the marine atmospheric surface layer for terms in the tke and scalar variance budgets', *J. Atmos. Sci.* **55**, 2311–2328.

Gent, P. R. and Taylor, P. A.: 1976, 'A numerical model of the air flow above water waves.', *J. Fluid Mech.* **77**, 105–128.

Harris, J. A., Belcher, S. E. and Street, R. L.: 1996, 'Linear dynamics of wind waves in coupled turbulent air-water flow. Part 2. Numerical model', *J. Fluid Mech.* **308**, 219–254.

Hsu, C.-T. and Hsu, E. Y.: 1983, 'On the structure of turbulent flow over a progressive water wave: theory and experiment in a transformed, wave-following co-ordinate system. Part 2', *J. Fluid Mech.* **131**, 123–153.

Hsu, C.-T., Hsu, E. Y. and Street, R. L.: 1981, 'On the structure of turbulent flow over a progressive water wave: theory and experiment in a transformed, wave-following co-ordinate system', *J. Fluid Mech.* **105**, 87–117.

Kitaigorodskii, S. A. and Donelan, M. A.: 1984, 'Wind-wave effects on gas transfer', *in* W. Brutsaert and G. H. Jirka (eds), *Gas Transfer at Water Surfaces*, Reidel Publishing Co.

Li, P. Y., Xu, D. and Taylor, P. A.: 1999, 'Second-order turbulence closure modeling for air flow over water waves', *J. Fluid Mech.* . submitted.

Lighthill, M. J.: 1962, 'Physical interpretation of the mathematical theory of wave generation by wind', *J. Fluid Mech.* **14**, 385–398.

Miles, J.: 1957, 'On the generation of surface waves by shear flows', *J. Fluid Mech.* **3**, 185–204.

Rhie, C. and Chow, W.: 1983, 'A numerical study of the turbulent flow past an isolated airfoil with trailing edge separation', *AIAA J.* **21**, 1525–1532.

Sullivan, P. P., McWilliams, J. C. and Moeng, C.-H.: 1996, 'A grid nesting method for large-eddy simulation of planetary boundary-layer flows', *Boundary-Layer Meteorol.* **80**, 167–202.

Zang, Y., Street, R. and Koseff, J. R.: 1994, 'A non-staggered grid, fractional step method for time-dependent incompressible navier-stokes equations in curvilinear coordinates', *J. Comp. Physics* **114**, 18–33.